Final Report
Asteroid Impact Monitoring

Environmental and Instrumentation Requirements

A component of the
Asteroid Impact & Deflection Assessment (AIDA)
Mission

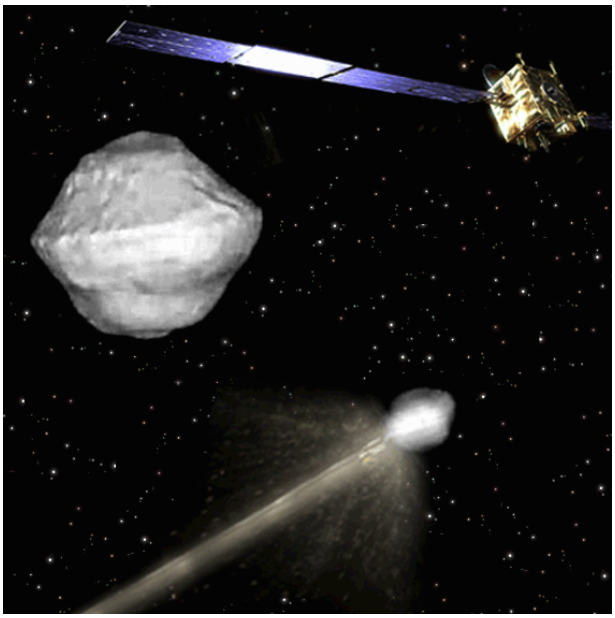

By the AIM Advisory Team

Dr. Patrick MICHEL (Univ. Nice, CNRS, OCA), Team Leader
Dr. Jens Biele (DLR)
Dr. Marco Delbo (Univ. Nice, CNRS, OCA)
Dr. Martin Jutzi (Univ. Bern)
Pr. Guy Libourel (Univ. Nice, CNRS, OCA)
Dr. Naomi Murdoch
Dr. Stephen R. Schwartz (Univ. Nice, CNRS, OCA)
Dr. Stephan Ulamec (DLR)
Dr. Jean-Baptiste Vincent (MPS)

April 12th, 2014

Introduction

In this report, we describe the knowledge gain resulting from the implementation of either the European Space Agency's Asteroid Impact Monitoring (AIM) as a stand-alone mission or AIM with its second component, the Double Asteroid Redirection Test (DART) mission under study by the Johns Hopkins Applied Physics Laboratory with support from members of NASA centers including Goddard Space Flight Center, Johnson Space Center, and the Jet Propulsion Laboratory. We then present our analysis of the required measurements addressing the goals of the AIM mission to the binary Near-Earth Asteroid (NEA) Didymos, and for two specified payloads. The first payload is a mini thermal infrared camera (called TP1) for short and medium range characterisation. The second payload is an active seismic experiment (called TP2). We then present the environmental parameters for the AIM mission.

AIM is a rendezvous mission that focuses on the monitoring aspects i.e., the capability to determine in-situ the key properties of the secondary of a binary asteroid. DART consists primarily of an artificial projectile aims to demonstrate asteroid deflection. In the framework of the full AIDA concept, AIM will also give access to the detailed conditions of the DART impact and its outcome, allowing for the first time to get a complete picture of such an event, a better interpretation of the deflection measurement and a possibility to compare with numerical modeling predictions.

The mission goal for the AIM study is twofold. On one hand it will provide the opportunity to demonstrate, on the minimum expression of a deep-space mission, technologies related to autonomous navigation, on-board resources management and close proximity operations. On the other hand it will characterise the secondary of a binary asteroid and demonstrate the technologies required by a simple monitoring spacecraft as well as establishing the suitability of binary asteroids as candidates for future explorations and asteroid deflection tests.

Both AIM and AIDA address issues that interest a large variety of communities, such as communities of researchers and engineers working on impact physics, planetary defense, seismology, geophysics (surface and internal properties), dynamics, mineralogy and resources, spectral and physical properties of small bodies, low-gravity environment and human exploration (see Fig. 1).

Several Work Packages (WP) have been defined. The first one (WP1) consisted in establishing and coordinating the AIM advisory team, and other organizational matters. Team member names are indicated on the cover of this report. This document reports the outcomes of the three other work packages defined for this study. WP2 corresponds to the analysis of required measurements addressing AIM mission goals, WP3 gives an environment analysis, and WP4 describes the knowledge gain resulting from AIM as a stand-alone mission and AIM in the framework of AIDA. For the sake of clarity we start by exposing the outcome of WP4.

I. Work Package 4: Knowledge gain resulting from AIM/AIDA

I.1. Knowledge gain resulting from AIM as a stand-alone mission

The characterization of the secondary of the binary asteroid Didymos will allow us to improve drastically our knowledge on the physical/compositional properties of at least a component of a Near-Earth Asteroid as well as to constrain formation scenarios of binaries. Having the same level of (or some) information regarding the primary would also be valuable to have a complete characterization of the system.

This knowledge is important for different reasons that are exposed below.

I.1.1. Mitigation strategies

There are several possible ways to deflect an asteroid, although none has been tested yet. All methods do not need the same amount of information regarding the targets. We indicate below a few examples (see Michel 2013, for more details).

Gravity tractor: mass is the fundamental parameter that is needed for the gravity tractor. Knowledge on rotational properties as well as shape is also important for proximity operations (especially if the tractor distance to the asteroid needs to be close).

Kinetic impactor: surface and sub-surface mechanical properties and porosity are the fundamental parameters that influence the outcome of a kinetic impactor mission. Size/shape properties are also needed for accurate targeting. As long as the area of the impact (and distance of shock wave attenuation from the impact point) is small compared to the whole body, the full internal structure does not need to be known.

Deployment of a device: surface and sub-surface mechanical properties are fundamental parameters for mitigation techniques relying on the deployment of a device on the surface (e.g. a solar sail).

Catastrophic disruption: if the impact energy may be close to the threshold for disruption (or if the aim is actually to disrupt the target), then some knowledge of the full internal structure (and global strength) becomes necessary.

Surface ablation: composition and thermal properties are needed for mitigation techniques relying on surface ablation.

I.1.2. Human exploration

The preparation of a human mission to an asteroid will rely on our knowledge of asteroid properties, in particular the mechanical properties at the surface and sub-surface, including regolith/dust properties, where an astronaut may interact, in a low-gravity environment. The presence of potentially hazardous moonlets (for an astronaut) and the amount/behavior of dust produced by an impact (e.g. micrometeorite) need also to be assessed. Rotational properties are also important to determine, especially to avoid fast-rotators.

I.1.3. Resource utilization

The possibility to use asteroids as resources needs a better knowledge on their detailed composition (mineralogy). Surface and sub-surface mechanical properties are also needed for the design of appropriate tools for material extraction.

I.1.4. Science.

AIM is not a mission devoted to science objectives. Here we just indicate that, scientifically, physical and compositional properties of small bodies provide crucial information on the history of our Solar System (see e.g. the rational for the MarcoPolo-R mission). In addition, the characterization of a component (secondary) of an asteroid binary (ideally of the full system) provides crucial information on the YORP spin-up mechanism at the origin of such a system and on its outcome.

I.2. Additional knowledge gain resulting from AIM within AIDA.

The implementation of the full AIDA mission will lead to unique information regarding the concept of the kinetic impactor as a deflection tool and the impact process itself. In effect, in addition to the knowledge gains resulting from the AIM mission as a stand-alone mission, if DART produces an impact on the secondary of Didymos, AIM will allow us:

- to interpret the resulting deflection in a way that is impossible if only ground observations measure the deflection;
- to observe for the first time the outcome of an impact on a small asteroid (e.g. the crater's size and morphology, the amount of ejecta), at a scale that is largely above what can be done in the laboratory.

Regarding the first item, AIM will contribute to access the initial conditions of the impact, e.g. the impact angle, and will relate the position of the impact point on the target measured by DART (within 1 meter accuracy, see Appendix) to the detailed properties of the whole object. This knowledge is crucial for our correct interpretation of the momentum transfer efficiency measurement. Moreover, although the deflection is planed to be observed from the ground, AIM will allow measuring it with greater accuracy and provide additional information about the binary system behavior after the impact.

Regarding the second item, AIM will provide unique knowledge on the impact process in the very conditions of an asteroid environment at a scale that is unreachable in the laboratory (limited to centimeter or meter-scale targets). For the first time, AIM will allow testing hypervelocity impact modeling and scaling laws at appropriate scale, and provide real data regarding the outcome, in terms of crater's size, morphology, as well as ejecta production and properties. This information will allow us to check or refine our impact modeling tools and scaling laws that can then be used with higher reliability to design other similar concepts in the future. It will also have a wide range of implications in planetary science, as the understanding of the impact response of a small body as a function of impact conditions and physical properties is crucial to estimate its collisional lifetime, the collisional evolution of

asteroid populations (when this knowledge is extrapolated to other bodies), and the role of collisions in various phases of our Solar System history.

So far, the only mission that performed such an impact was the Deep Impact mission (NASA) on July 4, 2005. However, the target was a comet, Tempel 1, 6 km in diameter, i.e. much greater than AIDA's target (150 meters in diameter), and the resulting crater could not be seen due to the unexpected big amount of fine ejecta. The STARDUST-NeXT mission (NASA) visited Tempel 1 much later, in 2011, after the comet passed its perihelion, but there is no clear guarantee that other processes did not affect the observed crater after such a long time, especially after a passage at close proximity to the Sun. The Hayabusa-2 mission (JAXA) to be launched in 2014 carries a Small Carry-on Impactor that will impact the primitive Near-Earth Asteroid 1999JU3 in 2018. However, the size of the projectile and the impact velocity (2 km/s) are designed to make a very small crater (order of a few meters, compared to the diameter of the object, around 800 meters) and not to produce a measurable deflection. Therefore AIM will be the only spacecraft that will observe the impact of a projectile in the impact speed regime that is both adapted to a deflection (technology demonstration) and consistent with the average impact velocities (about 5 km/s) between asteroids (science gain).

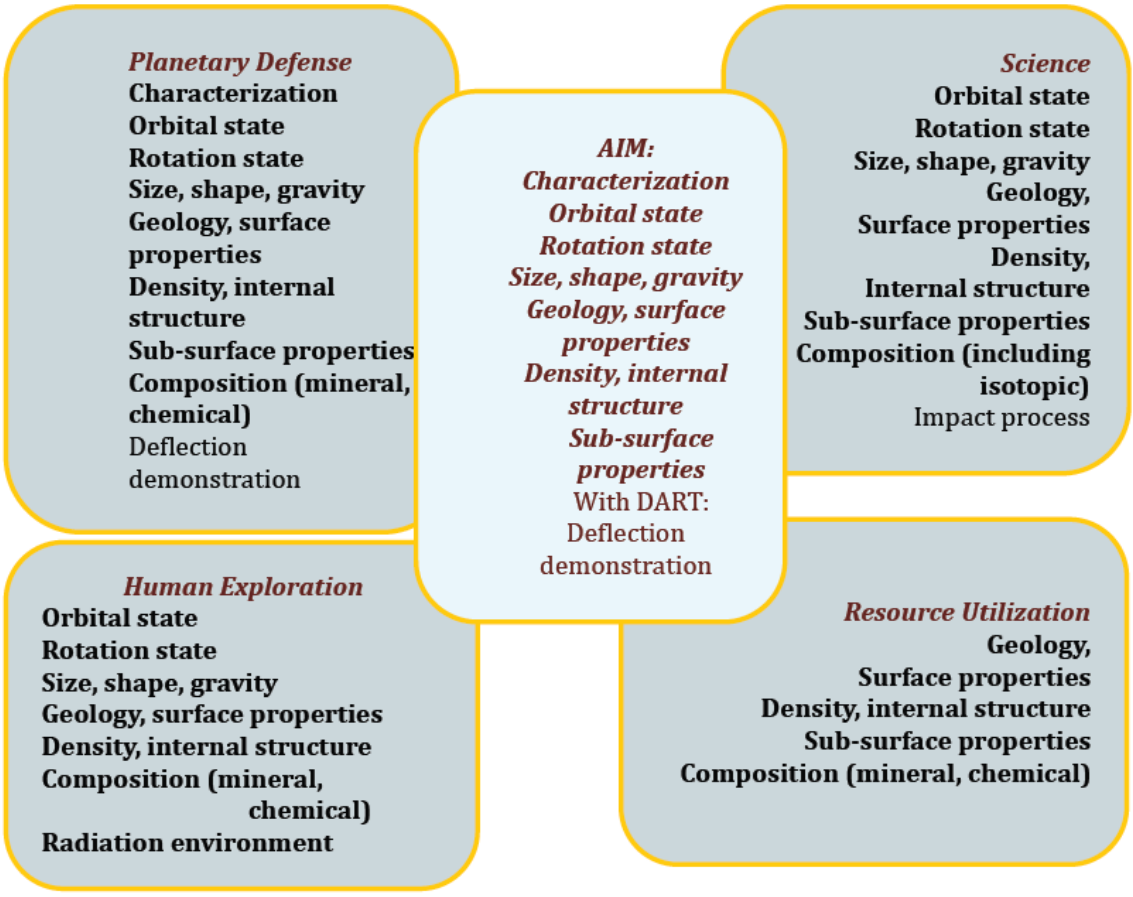

Figure 1: The full AIDA concept serves all NEO exploration stakeholders. The same applies to AIM as a stand-alone mission (bold characters), except for the deflection demonstration.

I.3 Summary of knowledge gain resulting from both concepts

Figure 1 shows that the full AIDA concept serves a wide range of objectives, as explained in previous sections. The same holds true for AIM (see Fig. 6, bold characters), except for the deflection demonstration.

II. WP 2: Analysis of required measurements addressing AIM mission goals

In this section, we identify the most relevant physical parameters to be measured as a function of the objective (e.g. planetary defense, resource utilization, etc) and formulate specific measurement technique requirements and margins. Accordingly we define a non-exhaustive list of payloads and requirements that can help in getting this information. Other instruments may exist that can help in achieving the mission goals and can be considered in a later stage.

The secondary of the binary asteroid is considered as the baseline target of the AIM mission with or without DART.

II.1. Objectives

In the following, we define two kinds of outputs from the measurements. First, we define mandatory outputs, and then other outputs whose importance depends on the objectives, as listed in Figure 1.

II.1.1. Mandatory and other outputs for AIM as a stand-alone mission

Images in the visible, the mass and surface (thermal and material) properties of the secondary, are mandatory (minimum) outputs of AIM, as they serve all four areas indicated in Fig. 1. Note that material properties can be derived either with a surface package and/or a thermal infrared camera, and/or exploiting the DART impact.

Other outputs that are required for specific objectives as listed in Fig. 1 are bulk compositional, physical and dynamical properties of the binary secondary.

Valuable outputs relevant to all areas: physical properties of the binary primary. A binary offers the possibility to improve our knowledge of two objects, instead of one, which is an advantage that could be exploited. Moreover, these two objects are linked by some processes at the origin of their separation. Having the possibility to get information about the primary would allow us to increase our understanding of such a system (15% NEAs are binaries) and its origin. In addition, a binary primary could also be the target of a future mission that may require information about such a body (e.g., for mitigation, resource utilization, human exploration).

II.1.2. Mandatory outputs in the framework of the AIDA cooperation mission (in *italics* in Table 1)

- Precise impact conditions (geometry/environment of the impact) of DART to interpret the deflection also measured by ground based observations.

- Physical properties of the secondary (impacted body) and their modifications after the impact (i.e. the characterization shall be carried out before and after the impact), the ejecta properties (size/speed), and the crater morphology.

The knowledge of the initial conditions and outputs of the impact will provide inputs and a test case for numerical models that can then be extrapolated to other cases.

- Orbital properties of the system and their changes after the impact (change in the orbit of the secondary around the primary).

Valuable outputs: compositional properties inside the crater formed by the impact (for resource utilization, science).

II.1.3. Compliance matrix

Table 1 lists the AIM parameters in relation with the measurement techniques required to measure those parameters.

Table 1: Compliance matrix of AIM objectives against measurement techniques (*in italics: relevant to AIDA only*).

Baseline objectives	Measurements	Payload (Examples)	Knowledge gain/relevant areas
Surface/ Sub-surface physical properties	Surface strength, porosity, density, mechanical properties, subsurface properties, thermal inertia	WAC/NAC + filters, impactor or hopper with accelerometer (interacting tool with the surface; e.g. penetrometer), in-situ imaging, Thermal Infra-Red spectrometer	Local properties, resource utilization, human exploration; Yarkovsky & YORP effects. *Momentum transfer (impact)*
Surface chemical, mineralogical properties	Elemental, chemical, mineralogical composition. Volatiles?	WAC/NAC + filters, Visible photometry, NIR spectrometer, in-situ IR spectrometer, APX/LIBS (on a surface package)	Compositional properties of a NEA; Resource utilization; *impact science (melting etc.); optional because of the "low" impact speed*
Global characteristics	Mass, shape, high resolution DTM, rotational properties, bulk composition, global subsurface properties, internal structure	Radio Science (RF-tracking), seismometers, radar sounding, LIDAR, WAC/NAC	CoG position; YORP; detailed physical properties of a NEA; *damping of impact energy*

Orbital parameters	State of binary orbit, heliocentric orbit	WAC, NAC Radio Tracking	Dynamical properties of a binary; *momentum transfer*
Impact event	*Dust production/properties* *Crater size/depth/morphology* *Composition in the crater*	*Dust monitor,* *Camera (stray light detection)* *IR spectrometer*	*Impact outcome* *Test of numerical models & scaling laws* *Sub-surface properties*

II.2. Measurement requirements

II.2.1. Surface/Subsurface Physical Properties

Measurements of mechanical properties of the surface and sub-surface are an important knowledge for the preparation of space missions aimed at interacting with the surface or at deploying a device. They can be derived either with a surface package and/or a thermal infrared camera, and/or exploiting the DART impact.

- Local properties (within a few cm depth) shall be measured at one random location (goal: measured at various (>2) locations):

- The average grain size shall be estimated within an order of magnitude (goal: estimation of size distribution from 1 μm to 100 m, i.e. regolith to boulders).

- It shall be possible to discriminate between various classes of porosity[1] (<20%; 20-50%; 50-80%; >80%).

- It should be possible to measure the elemental composition of surface material in at least one area, both mixing elements (Na <-> Ni) and light elements (most importantly CNO).

- Local properties (within a few meter depth) should be measured at one random location (goal: measured at various (>2) locations):

- The speed of sound (P-wave) should be measured within an accuracy of 50% (goal 10%).

- The speed of the S-wave in the subsurface should be measured within an accuracy of 50% (goal: 10%).

- The tensile strength should be measured within an order of magnitude (goal 20% accuracy).

[1] Note: porosity is given by porosity=1-(ρ/ρ_s), where ρ is the bulk density and ρ_s the grain density. The precision of the porosity depends strongly on the values and precisions of ρ and ρ_s.

- The compressive strength should be measured within an order of magnitude (goal 20% accuracy).

- The sub-surface (~10m depth) should be characterized at one site to provide information on heterogeneities (of m-size) (goal: 3 sites to provide information on heterogeneities).

II.2.2. Global Characteristics

- For the purpose of volume estimation, a closed shape model shall be obtained with an accuracy of typically 1 m in both height and spatial resolution with respect to the center of mass.

- The mass of the secondary shall be determined with an accuracy of 10%[2] (goal: 1%).

- The resolution of surface images shall be better than a meter/pixel (goal: the DTM shall have a resolution of 1 m lateral and 0.3 m vertical resolution - pixel resolution must be factor 3-5 times better, depending on method.)[3]

- The surface temperature of the complete target shall be derived to an accuracy of at least 5 K (goal 1 K) above 200 K (goal: 150 K). The spatial resolution shall be of the order of a meter at a number of rotational phases and times of the day. This will allow the thermal inertia to be determined to a precision of better than 10 %.

- The complete surface of the target should be imaged in at least 3 different colours, in the visible range.

- The complete surface of the target shall be imaged in the visible.

- The complete surface of the target should be imaged in the near-IR wavelength range from 0.4 to 3.3 μm and with a mean spectral resolution of $\lambda/\Delta\lambda$ of the order of 200 and a spatial resolution (= twice the pixel scale) of the order of metres to characterize the mineral properties of the surface.

- The complete surface of the NEA should be imaged in the mid-IR with a spatial resolution of the order of 10 m or better and with a spectral resolution of $\lambda/\Delta\lambda$ of the order of at least 200 to determine the wavelength dependent emissivity, and hence identify mineral features in the range 8 – 16 μm (goal 5 – 25 μm).

Note: it is acknowledged that depending on the rotation axis of the asteroid there may be areas that cannot be imaged during the global characterization phase due to illumination constraints.

---

[2] This accuracy allows the measurement of the beta factor, from a deflection, with enough accuracy for comparison with beta factor estimates through modeling.

[3] DTM has two main purposes: 1- to assess morphology changes by measurements before and after the impact, as well as to determine the boulder size distribution; 2- to measure the small scale topography to increase the accuracy of the YORP effect estimate.

- The inner structure of the secondary should be constrained before and after the impact (in the framework of AIDA), with the goal of doing this to a depth down to the center of the body and a spatial resolution of about 10 m.

- It should be possible to detect the presence of volatiles.

- In the framework of AIDA, it should be possible to perform those measurements within the crater.

- In the framework of AIDA, the rotational excitation of the secondary should be measured. A change at the level of $3x10^{-8}$ rad/s (about a degree per week) should be measurable.[4]

II.2.3. Orbital parameters (AIDA framework only)

Orbital parameters shall be measured before and after the impact. The level of accuracy depends on the mission scenario for AIM orbital operations, and how well the AIM position and attitude will be determined.

Assuming that AIM adopts a similar scenario as the Hayabusa scenario (distant home position), then from images of the two bodies:
- it shall be possible (within weeks) to determine semi-major axis to 0.1%
- it shall be possible (within weeks) to detect any inclination change at the milliradian level.
- The eccentricity before and after the impact should be measured with sensitivity about 0.002.

II.2.4. Impact outcome (AIDA framework only)

- The size distribution of the ejecta should be measured along one line of sight (goal: 3 lines of sight) from the largest down to < 10 microns.

- The ejecta cloud shall be monitored for a few weeks to infer the ejecta velocity field properties.

- Crater size and morphology are already accounted for in the global property measurements.

- A seismometer (using as a source DART impact) should provide information on the internal and subsurface properties.

II.3 Requirements for a Micro Thermal Infrared Camera (TP1)

The micro thermal infrared camera is assumed to be a low mass, low system impact instrument that can be used in planetary missions for e.g. whole body IR emission, rough assessment of surface temperature gradient, and, ideally, assessment of dust and environment around the body. Here we provide a set of simple requirements

[4] This would be very useful, as it can be compared to the angular rate corresponding to velocity change of 0.1 mm/s at a moment arm of 100 m, which would be $1x10^{-6}$ rad/s.

adapted for utilization on a small body (that can be scaled to other possible applications).

A spectroscopic mode is note required.

For the detectors: a microbolometer focal plane array is suggested (http://www.flir.com/cvs/cores/view/?id=62648).

Space qualification is required.

A Radiation damage study is required (see, e.g. https://www.researchgate.net/publication/224362473_Radiation_Effects_in_InGaAs_and_Microbolometer_Infrared_Sensor_Arrays_for_Space_Applications).

The camera should be capable of operating for several years in space.

The wavelength range shall be between 8 to 14 μm, 5 to 20-25 μm is desirable (note that microbolometers are typically working between 8 and 14 microns).

The Temperature range shall be: maximum 400 K, minimum 200 K (desirable minimum 150 K). This range is required to be able to measure the day and the night side of an asteroid.

Absolute temperature accuracy: 5 K (desirable 1K between 500 and 200 K; the accuracy can be lower between 200 and 150 K). This is to see the temperature contrast to measure regolith temperature variations due to the thermal inertia.

The sensitivity is specified by the temperature accuracy and the temperature range indicated above.

Calibration: linearity of the response. If not linear, the stability of calibration curve should be given.

Dynamic range is specified by the temperature range above or at least 10,000.

The spatial resolution on the asteroid surface shall be about 1 m from a few km away from the surface. Given that the angular resolution θ is equal to λ/D, where λ is the wavelength and D is the aperture diameter, then for $\theta \sim 10^{-3}$ radians, at $\lambda=10$ μm an aperture of 1 cm is enough to achieve that resolution.

A minimum requirement of 640x480 pixels is indicated for the size of the array. For instance, microbolometre arrays of 640x480 exist from the shelf - typical pixel size is 15-20 μm; with 2 cm focal length, a 1m pixel at 1 km is achieved.

A larger array, such as 1k x 1k is desirable to have a Field Of View covering the whole disk of an asteroid of about 800 m of diameter from 1 km of distance.

II.4. Requirements for the seismic experiment (TP2)

The seismic experiment is assumed to be a low mass, low system impact instrument that can be used in modest planetary missions to determine in-situ fundamental physical properties and the internal structure of the body. It is assumed to consist of a surface package (seismometers) and an active source. However, such an experiment is highly constrained by the considered application (e.g., the Moon or a planet, versus a small asteroid). Here we provide a set of simple requirements adapted for utilization on a small body.

- The frequency range shall cover at least 100 Hz to 200 Hz.

- The speed of sound (P-wave) shall be measured within an accuracy of 50% (goal 10%).

- The speed of the S-wave in the subsurface should be measured within an accuracy of 50% (goal: 10%).

- The sub-surface (~10m depth) should be characterized at one site to provide information on heterogeneities (of m-size) (goal: 3 sites to provide information on heterogeneities).

For further study of this payload, we give a set of recommendations:

- The surface acceleration produced globally by an active source should be estimated as function of the type and energy of the source, the distance from the source, and a range of simple structural representations of the object (e.g., assumed global Q factor). An appropriate sensitivity of the instrument shall be defined on this basis.
- A trade-off shall be made between a number of active sources versus a number of sensors.
- The coupling between the seismometers and the surface shall be investigated. Solutions shall be proposed or consequences shall be described if coupling is found to be uncertain.
- An analysis of system level impacts of this experiment could be considered (e.g., telemetry challenges due to the large volume of data).
- Alternative methods to seismometers to measure the acceleration could be considered (e.g. detecting regolith motion following the active impact with a high-speed camera).

III. Work Package 3: Environment analysis

III.1. Before the impact

The following describes our current knowledge of the environment faced by AIM as a stand-alone mission, or before the impact performed by the DART projectile.

III.1.1. Target properties

The target is the secondary of the binary asteroid 65803 (1996 GT) Didymos, an Apollo asteroid (perihelion distance smaller than 1.017 AU, semi-major axis greater than 1 AU) discovered on April 11, 1996 by Spacewatch at Kitt Peak. It has a satellite orbiting it with a period of 11.9 hours, hence the appellation "Didymos", meaning "twin".

Known parameters of Didymos are:

- Semi-major axis: 1.644 AU
- Orbital (heliocentric) period: 770.14 days
- Eccentricity: 0.384
- Inclination: 3.4 deg.
- Geometric albedo: 0.147.
- Primary rotation period: 2.26 hr
- Diameter of the primary: 800 m.
- Diameter of the secondary: 150 m.
- Orbital period of the secondary: 11.91 h (almost circular orbit).
- Separation: 1100 m.
- Binary orbit semi-major axis: 1050 m
- Orientation of the mutual orbital plane is known (2 solutions)
- Pole Solutions (lambda, beta) = (157 deg., 19 deg.); (329 deg., -70 deg.)

Thanks to a close approach of the asteroid to the Earth in November 2003 (0.048 AU on Nov. 12, 2003), radar observations were performed by Goldstone and Arecibo (see Fig. 2). Note that radar data cannot provide a model of the secondary: the SNR is too weak, echoes are not sufficiently resolved, and the rotation coverage is limited. The dimensions, mass and density of the secondary are not well constrained. Secondary bandwidths and visible extents are consistent with synchronous rotation. The radar albedo is consistent with silicates and inconsistent with pure metal. Near-surface roughness is lower than the NEA average and somewhat less than on Eros, Itokawa, and Toutatis.

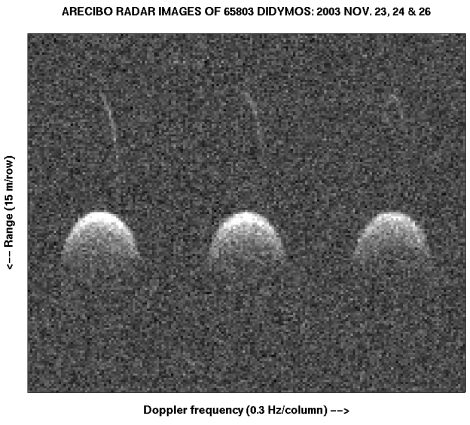

Figure 2: Radar observations of Didymos performed by Arecibo in November 2003.

Regarding its spectral properties, Didymos is now classified as an S-type (DeLeon et al. 2010), even if it was originally classified as an Xk-type (Binzel et al. 2004) due to limited wavelength coverage. Figure 3 shows the spectrum obtained by DeLeon et al. (2010) compared with that of two visited Near-Earth Asteroids, namely (433) Eros

and (25143) Itokawa. Thus, Didymos belongs to the most common NEO type. The only educated guess regarding its properties comes from a comparison with the properties of the two visited NEAs of the same type: Eros and Itokawa. In particular, samples have been returned from Itokawa, whose properties are similar to those of thermally metamorphosed LL chondrite meteorites. More precisely, the mean compositions of grains of the iron-magnesium silicate minerals olivine and pyroxene fall squarely in the range of those in LL ordinary chondrite meteorites.

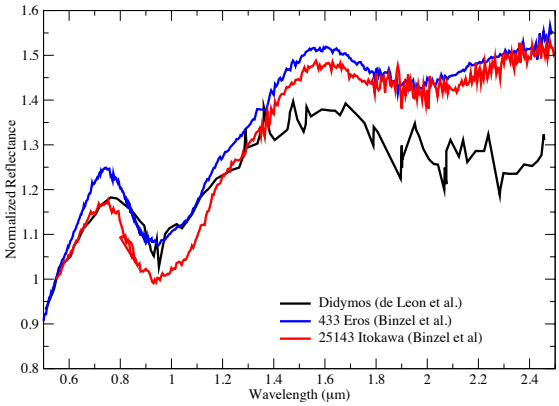

Figure 3: spectrum of Didymos (black) compared with that of Eros (blue) and Itokawa (red).

III.1.2. Observational opportunities

Table 2 indicates the main facilities that may be used to observe Didymos. Existing 2-m class telescopes can only be used during the period when the asteroid is brighter than ~21st magnitude. Observations in April 2015 should allow the pole position to be better constrained. Ground-based NASA assets can be used as appropriate, noting that some are easier to schedule (IRTF) than others (Keck). HST observations can be made when the asteroid is fainter and closer to the Sun (>50 degrees). It should also be possible to involve the Magdalena Ridge Observatory expertise, non-US observers, as well as amateur astronomers. One plan will be to contact leaders of similar campaigns (Deep Impact, etc.) for lessons learned.

No radar observations can be performed until 2022. During this apparition, Didymos will be observable at Goldstone starting on Sep. 29 and at Arecibo starting on Oct. 24. Goldstone SNRs will be ~1/4 of those in 2003. It will be able to detect the primary and possibly the secondary with Continuous Wave (CW) observations. Ranging of the primary will be possible but no detailed images. No images of the secondary will be obtained either. Arecibo SNRs will be ~30% as strong as in 2003 but seven times stronger than at Goldstone. Imaging at 75 m resolution and possibly 30 m will be performed, with weak detections of the secondary. It will be primary detectable at Goldstone until early November and at Arecibo until late December.

The astrometric mission Gaia (ESA) might detect Didymos in March 2019, but only marginally. Indeed the visual magnitude of the binary asteroid will be $V_{Didymos}$~19.8, which is almost at the limit of Gaia capability (V=20). There is another opportunity in 2020 with $V_{Didymos}$~19.7, provided that Gaia operations are extended to six years, while the nominal mission has a five-years duration. In order to calculate the visibility

from Gaia, the final scientifically scanning law must be defined, which will happen by the end of May 2014.

VLTI will not observe Didymos until the close approach of September 2022, when $V_{Didymos}$~14. Then, VLTI (with the instrument MATISSE) will be able to resolve the two components when their angular separation will be around 30-50 mas and the asteroid will be bright enough for fringe detection in the N, L and M bands.

Table 2: Ground facilities for the observations of Didymos (compilation by A. Rivkin, JHU/APL).

Facility	Use	Notes
Small (1-2 m) telescopes	Light-curves at some times, imaging	National facilities/University facilities
NASA IRTF (3 m)	Light-curves, spectroscopy, imaging	Goal to support NASA missions
Apache Point Observatory	Light-curves, imaging	JHU/APL has (small) share
Keck Observatory (10 m)	Imaging	NASA has small share
Hubble Space Telescope	Light-curve? Imaging	Probably defunct by impact
ALMA	Sub-mm imaging	Might separate components
Spitzer	Imaging, physical properties	
JWST		Cannot track NEOs
WISE	Physical properties	"Might get in 2015". Defunct by 2018. Not pointable.
Gaia	Astrometry	ESA mission
Pan-STARRS/LSST	Imaging?	Unclear if pointable. Not obviously useful.
Radar	Imaging, satellite detection	S/N>30 only Aug-Dec 2022
Gemini AO	Imaging	Maybe separate components?
Magdalena Ridge Obsevatory	Light-curves, imaging	Specialized in NEO light-curves.

III.1.4. Unknown properties

Many properties cannot be known in advance at least not in great detail, but for some of them some expectations can be established based on current knowledge and modeling work. AIM will then allow our predictions to be tested.

III.1.4.1. Main physical properties

A refined shape model will not be obtained before the encounter. Further work regarding the modeling of YORP spin-up may provide some constraints. Recall that the YORP effect is a thermal effect that can increase or decrease the rotation period of an asteroid whose shape is not perfectly spherical. In particular, YORP spin-up can lead to migration of material from the pole to the equator, turning an almost spherical object into an oblate spheroid with an equatorial ridge. Understanding of this process can allow the determination of the possible evolution of the shape of an object as a function of its thermal properties and other relevant physical/dynamical properties.

The mass and possibly size of the secondary, and consequently the density difference between the primary and secondary, will not be known in advance. The same holds true regarding detailed surface properties as well as any knowledge on the internal structure and spectral properties in the infrared. However, based on our understanding of binary formation by YORP spin-up, it is likely that both the primary and secondary of Didymos are gravitational aggregates (Walsh et al. 2008, 2012), although given the fast rotation period of the primary, some cohesion is expected (see Sec. III.1.4.3). In particular, the secondary could be formed by reaccumulation of small pieces escaping the primary during YORP spin-up. The primary may also be richer in regolith at its equator.

III.1.4.2. Thermal properties

Regarding thermal properties, the thermal inertia will not be known in advance. More precisely, from the ground, the asteroid needs to be at magnitude 18 or below to have thermal IR measurements, which will only happen in 2022. From space, measurements can be done provided that JWST is launched in 2018 (or 2019). From the approach phase during the AIM mission, the thermal inertia can be measured with a thermal camera, but the spacecraft needs to be a few hundreds of kilometers away from the target or closer.

Figure 4 shows a preliminary temperature distribution at the surface of the asteroid Didymos (primary) calculated at 1.664 AU from the Sun for a thermal inertia of 100 J m^{-2} $s^{-0.5}$ K^{-1}, bolometric Bond albedo of 0.1, emissivity of 0.9 and assuming that the asteroid spins perpendicular to the direction toward the Sun, which is not necessarily the case given the obliquity of the asteroid (Pravec et al. 2006).

The radar shape of the asteroid 1999 KW4 (downloaded from http://echo.jpl.nasa.gov/asteroids/shapes/kw4a.obj) is assumed (prolate spheroid), and scaled such that the equivalent volume diameter is that of Didymos, i.e. 800 m.

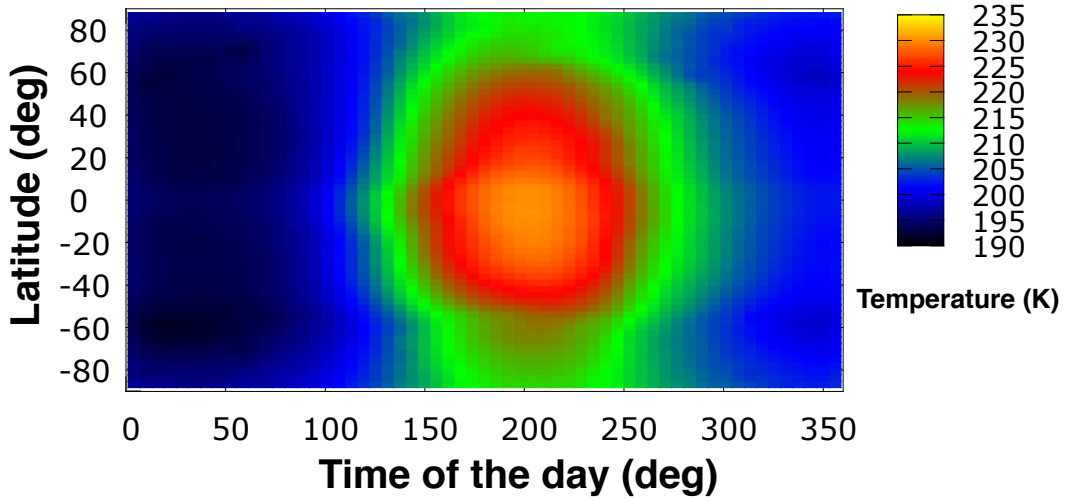

Figure 4: Preliminary temperature distribution at the surface of the asteroid Didymos calculated at 1.664 AU from the Sun (see text for details). Local midnight corresponds to 0 degrees. The hottest spot is not at 180 degrees (noon), but is slightly shifted because of the thermal inertia.

Given the temperature distribution, the thermal model allows one to calculate the flux towards the spacecraft, including the reflected light component. Figure 5 shows the spectral energy distribution (SED) at the distance of 1 km to the asteroid.

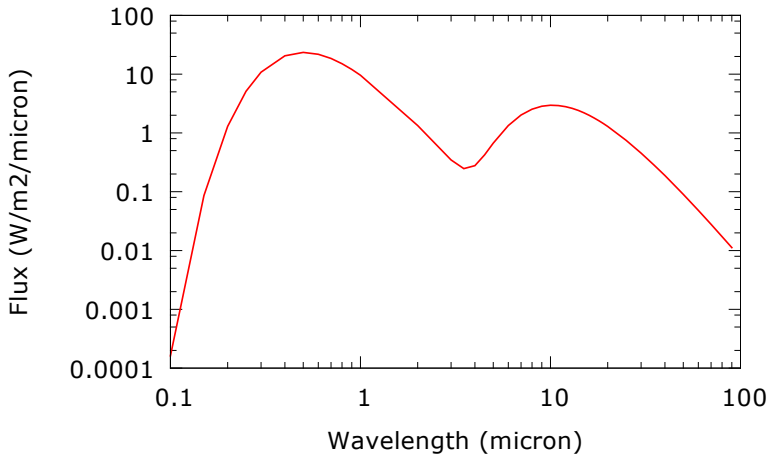

Figure 5: Spectral energy distribution (SED) at the distance of 1 km of the asteroid.

The total power from the asteroid and thus heating the spacecraft is given by the integral of the SED, which gives about 66 W/m^2. Assuming the spacecraft absorbs this radiation entirely and has an emissivity of 0.5 this gives a temperature of $(66/6.67\text{x}10^{-8}/0.5)^{0.25}$ i.e. ~210 K. The temperature is proportional to the inverse square root of the distance to the asteroid.

III.1.4.3. Environment between the two components

By definition, an asteroid binary is composed of two main bodies, a primary and a secondary. However, the possible existence of dust and boulders evolving between

the two components must be assessed. Binary systems like Didymos are understood to form as a result of the thermal YORP spin-up of a single object (see discussion in Sec. II.1.4.1). During the secondary formation, mass transfer from one body to the other does happen. However, once the secondary is formed and when it is stabilized, which results in its rotation state being spin-locked, then no major mass transfer is expected to have occurred recently. Didymos is now in this state, with its secondary spin-locked. However the primary's rotation is about 2.26 hrs. In fact, the case of Didymos is very interesting. The primary is actually above the spin limits for a cohesionless body, by about 30% (unless its density is >3 g/cc). But its surface speed is below its escape speed. Didymos' primary is one of the largest of the "fast spinners" just below the 1km size but above the limit for a purely gravitaty-dominated body. Thus, it must have some global cohesion (Holsapple, private communication). Note that for any body spinning above the rubble-pile (gravity) limit, the surface velocity is greater than the orbit speed at the equator. Consequently, loose surface particles will be lifted from parts of the surface (especially from the furthest radius of the equator). That can happen any time loose particles are created, e.g. by impacts or thermal cracking (Delbo et al. 2014). In addition, the tidal pull of the secondary can create additional perturbations known as "tidal saltation" (Harris et al. 2009). Then, as long as the surface speed is less than the escape speed, a lifted particle will not escape, but will orbit the primary for a time that needs further studies to be determined. It may be that their long-term fate is to join the secondary or to rejoin the primary at a different location.

In summary, all asteroids (including Didymos) spinning between omega=$(4 \text{ Pi rho } G/3)^{1/2}$, where rho is the bulk density and G the gravitational constant, and $(8 \text{ Pi rho } G/3)^{1/2}$ can be expected to have at least temporary orbiting debris; the fate of those debris is complicated, but under study (Holsapple, private communication).

Note that asteroids spinning faster than that upper limit will have no coarse surface regolith (but fine dust may have enough cohesion to remain on the surface). Those in-between may have regolith only on parts of the surface.

Regarding small dust particles, their survival is very short before migrating to the Sun due to radiation forces. Therefore, unless a mechanism was identified to cause a sufficiently continuous dust production to maintain some quantity between or in the vicinity of the system, it is reasonable to assume that dust will not be a threat for the mission (shutters for the camera may be envisaged, especially in the framework of AIDA).

III.1.4.4. Possible Yarkovsky drift (and implication on thermal inertia)

In recent years, several works derived the density of NEAs by comparing measurements of the rate of change of the orbital semi-major axis *da/dt* due to the Yarkovsky effect with model predictions of the same observable, the latter being dependent on the size, shape, pole direction and rotation rate of the asteroid as well as the value of the thermal inertia and object's bulk density (Chesley et al. 2014, Rozitsis and Green 2013, Rozitsis et al. 2013).

In the case of Didymos, in principle the same approach could be used do derive the value of the thermal inertia, assuming that all other parameters were known. In fact,

this is the only way that can be used for now to derive this parameter as there is little possibility of performing thermal infrared observations before 2022.

III.1.4.5. Mineralogical environment

Considering that 1) Didymos is classified as an S-type (DeLeon et al. 2010), 2) Didymos belongs to the most common NEO type, 3) Dydimos spectral characteristics resemble those of Itokawa, 4) the mineralogy and mineral chemistry of the Itokawa samples are identical to those of thermally metamorphosed LL5-LL6 chondrites, we review here the main characteristics of ordinary chondrites with some specific emphasis on LL chondrites (Fig. 6), which may constitute an appropriate mineralogical environment.

Constituents of ordinary chondrites

Corresponding to the most populated group of chondrites (85% of meteorite falls), ordinary chondrites are commonly subdivided in three subtypes according to the amount of total iron, of iron metal and iron oxide in the silicates: H (46%), L (40%) and LL (10%).

Figure 6: Example of Ordinary chondrite: Krymka LL3.2 , Fall, Ukraine. (Credit: Meteorite times magazine).

In ordinary chondrites, chondrules are the main constituent by far with 60-80 vol% (Fig. 7). They are cemented by a thin matrix (10-15 vol%). Metal and sulfides are present in various proportions depending on the subtype. By comparison to carbonaceous chondrites, refractory inclusions are rare.

PETROGRAPHIC CHARACTERISTICS OF THE CHONDRITE GROUPS

	Chondrule abundance[1] (vol%)	Matrix abundance (vol%)	Refractory inclusion abundance[2] (vol%)	Metal abundance[3] (vol%)	Chondrule mean diameter (mm)
CI	<<1	>99	<<1	0	-
CM	20	70	5	0.1	0.3
CR	50-60	30-50	0.5	5-8	0.7
CO	48	34	13	1-5	0.15
CV	45	40	10	0-5	1.0
CK	15	75	4	<0.01	0.7
CH	?70	5	0.1	20	0.02
CB	3-10??	?	?	40?	
H	60-80	10-15	0.1-1?	10	0.3
L	60-80	10-15	0.1-1?	5	0.7
LL	60-80	10-15	0.1-1?	2	0.9
EH	60-80	<2-15	0.1-1?	8	0.2
EL	60-80	<2-15	0.1-1?	15	0.6
R	>40	36	0	0.1	0.4
K	27	73[4]	<0.1	0[4]	0.6

[1]Chondrule abundance includes mineral fragments.
[2]Refractory inclusion abundance includes CAI + AOI.
[3]Metal abundance is for metal outside chondrules.
[4]Matrix abundance includes metal.
Abundance sums of les than 100 vol% are because of significant sulphide component in most cases.
Sources: Scott et al. (1996) except for CO data (McSween, 1977a), K (Kakangari) chondrite data (Weisberg et al., 1996), and "CH" (ALH85085) chondrule mean diameter from Grossman e t al. (1988a) and Scott (1988).

Figure 7: Petrographic characteristics of the chondrite groups

Chondrule size in ordinary chondrites is on average below 1mm, but varies markedly according to the ordinary chondrites subtypes from 0.3mm in H chondrites, 0.5 in L and to around 0.6 in LL (Fig. 8).

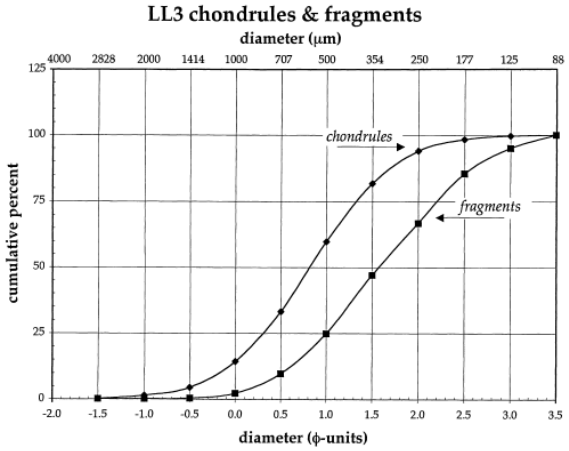

Figure 8: Cumulative size frequency diagram for chondrules and fragments in five LL3 chondrite (Nelson and Rubin, 2002)

Metal and iron sulfide grains are well smaller. While the masses of the chondrules were found to vary between chondrite groups similar to the trend established for chondrule sizes, i.e., decreasing from LL to L to H, the sizes and masses of the metal–troilite grains were found to increase in this sequence.

Mineralogy of ordinary chondrites

Mössbauer spectroscopy and X-ray diffraction have been used to quantify the modal mineralogy of unequilibrated ordinary chondrites (UOCs) and equilibrated ordinary chondrites (EOCs) by Menzies et al. (2005) and Dunn et al. (2010) (see Fig. 9-10).

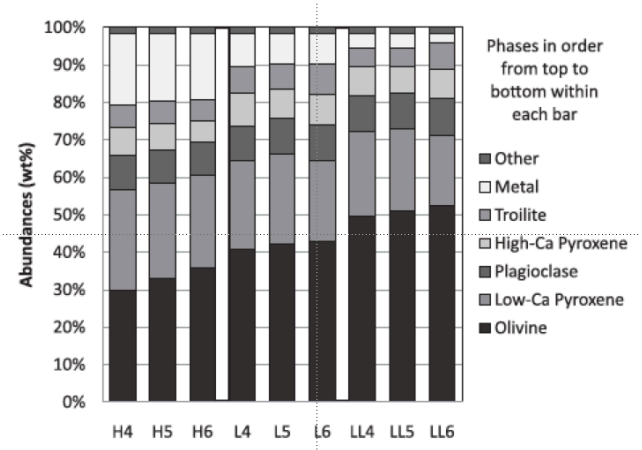

Figure 9: Modal mineralogy in equilibrated ordinary chondrites; trend from 4 to 6 indicating increasing thermal metamorphism.

EOCs are comprised primarily of olivine and low-Ca pyroxene (50–75 wt% total), with some high-Ca pyroxene, plagioclase, metal, and troilite. Olivine abundances increase from the H to the LL chondrites, whereas low-Ca pyroxene and metal abundances decrease. High-Ca pyroxene, plagioclase, and troilite abundances are relatively consistent between the three ordinary chondrite groups.

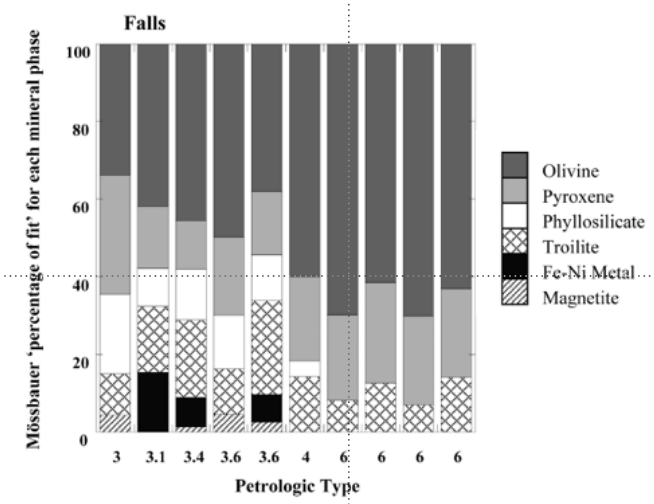

Figure 10: Modal mineralogy in LL unequilibrated ordinary chondrites (UOCs) from 3 to 3.6 compared to LL equilibrated ordinary chondrites (EOCs) with increasing thermal metamorphism.

UOC are dominated by the ferromagnesian silicates: olivine and low-Ca-pyroxene. All of the samples contain a paramagnetic phase indicative of a ferric-bearing phyllosilicate, e.g. clay like. This phase clearly decreases in abundance with metamorphism, an inverse relationship to that observed for both olivine and pyroxene. The suggestion is that dehydration of phyllosilicate occurred with progressive metamorphism to produce ferromagnesian silicates. Krot et al. (1997) have shown that fayalitic olivine in CV3 chondrites could be formed by aqueous alteration of ferromagnesian silicates and subsequent dehydration of phyllosilicates within the parent body.

Density and porosity of ordinary chondrites

Wilkinson et al. 2002 measured the porosity and the density of a set of ordinary chondrites. and are summarized in the Table 3.

Table 3: average porosity density values for the H, L and LL groups.

Table 2. Average porosity and density values for the H, L, and LL groups.

Meteorite group	n	Weighted average grain density (g/cm^3)	Average bulk density (g/cm^3)	Weighted average porosity (%)	Average porosity (%)	Porosity range (%)
H	15	3.67 ± 0.04	3.39	8.3 ± 1.0	6.9	0–27
L	21	3.39 ± 0.03	3.31	3.7 ± 1.0	1.7	0–14
LL	6	3.44 ± 0.05	3.28	8.0 ± 1.7	7.5	0–18

Interestingly, they have shown that no relation exits between porosity and metamorphic grade, chemical group, mass, density, or shock level among ordinary chondrite meteorites.

III.1.4. 6. Electromagnetic environment

Objects in space charge to a floating potential determined by the balance between charging currents in the local plasma environment (Whipple et al. 1981, Goertz et al. 1989). The dominant currents are the flux of electrons and ions from the ambient plasma, the electrons created by secondary emission and the photoelectrons. The charging of a surface in space will proceed until the sum of the charging currents is zero and the object has reached an equilibrium floating potential (Sickafoose et al. 2000). Such surface charging has been observed on the Moon with the night side surface reaching potentials of up to -4.5 kV (Halekas et al. 2009) and has been known to cause the lunar dust to levitate (Colwell et al. 2007). It has been speculated that a similar mechanism may cause levitation and transport of grains on the surface of an asteroid (Lee et al. 1995, Colwell et al. 2005, Hughes et al. 2008). It is, therefore, likely that electrostatic forces may occur on the surface of asteroids. However, no in-situ electrostatic measurements have been performed at the surface of an asteroid. So, occurrence of electrostatic forces cannot be assessed in the case of Didymos but should be kept as a possibility.

III.1.4.7. Expected meteoroid flux

Expected meteoroid flux that may be used as a source of seismometers can be estimated on the basis of estimates of the frequency that cometary micrometeoroids (the dominant flux) impact an asteroid's surface. Such an estimate is given in Delbo et al. (2014, section Method).

III.1.5. Other known binaries

Using the Minor Planet Physical Properties Catalog (mp3c.oca.eu), we selected all binary asteroids having sizes of the primary smaller than 10 km and belonging to the spectroscopic S-complex (S, Sr, Sq, Sa, Sl in the SMASS II, Tholen or DeMeo-Carry taxonomies). 22 asteroids matching those criteria are found in the database (see Table 4). Note that we did not include in the search binary asteroids having a different

taxonomic class or a low albedo, as these bodies might not be good proxies for Didymos.

Table 4: Binary asteroids belonging to the S-complex with primary's size smaller than or equal to10 km (source: http://mp3c.oca.eu). All sizes and albedos are provided by NEOWISE, except those indicated in red (source: http://earn.dlr.de).

Name	D (km)	p_V	Mag H	a (AU)	e	i (deg)
(1052) Belgica	10.40	0.273	11.97	2.2355853	0.143673	4.6958
(1139) Atami			12.51	1.9474773	0.2554135	13.0857
(1830) Pogson	8.28	0.236	12.45	2.1882576	0.0559695	3.95422
(1862) Apollo	1.40	0.26	16.25	1.470083	0.559992	6.35279
(1866) Sisyphus	7.64	0.224	12.40	1.8937266	0.538332	41.19205
(2131) Mayall	8.55	0.198	12.72	1.8871758	0.1110836	33.99543
(2478) Tokai	9.98	0.208	12.00	2.2252566	0.0684265	4.13775
(2754) Efimov			13.60	2.2284303	0.2319537	5.71147
(3309) Brorfelde			13.60	1.817707	0.0532149	21.13295
(3873) Roddy			12.70	1.892227	0.1338005	23.35525
(4029) Bridges	7.73	0.216	12.80	2.5252045	0.1308456	5.4372
(4951) Iwamoto	5.51	0.185	13.20	2.2569809	0.1666592	7.52818
(5905) Johnson	4.79	0.193	14.00	1.9103521	0.0718245	27.52208
(6265) 1985 TW3	4.95	0.286	13.40	2.1661301	0.1931586	4.11417
(7225) Huntress	6.68	0.165	13.00	2.3410297	0.20316	6.87171
(15268) Wendelinefroger			14.60	2.365251	0.2350196	2.75404
(15700) 1987 QD			14.60	2.2087322	0.3160163	26.77631
(17260) 2000 JQ58			14.20	2.2046077	0.1832252	5.28349
(26471) 2000 AS152	6.05	0.30	13.20	1.9177657	0.1544784	19.69397
(31345) 1998 PG			17.30	2.0151595	0.391533	6.4941
(99913) 1997 CZ5			13.40	2.2938788	0.3971487	24.90214
1994 AW1			17.50	1.1047529	0.0754141	24.1001

III.2. After the impact:

III.2.1. Change in physical properties of the secondary

The impact will produce a crater on the secondary. Its size and morphology highly depend on the internal structure and mechanical properties of the secondary. Numerical simulations of hypervelocity impacts with a 3D Smooth Particle Hydrodynamics (SPH) hydrocode using the impact conditions of DART and assuming a porous structure of the secondary were performed. They indicate that the diameter of the crater may be of the order of 15 meters. Other structures would lead to a different size. Large-scale restructuring is unlikely to occur given the size of the impact event compared to the size of the whole body. On the other hand, regolith displacement may occur in the vicinity of the impact point and crater, due to the very low gravity of the asteroid that may cause even small seismic waves to move or lift off loose material. However, there are no reliable existing tools and knowledge to quantify these effects.

III.2.2. Change in dynamical properties of the secondary and primary

The dynamical properties will be affected by the impact. In particular, the orbit of the secondary around the primary will be modified, as well as possibly its rotational properties. As a consequence the dynamics of the whole system will be affected in a way that cannot be assessed at the present stage. Assuming a porous structure the so-called beta factor (momentum of the projectile + momentum of the ejecta in the opposite direction of the impact, normalized by the momentum of the projectile) is 1.4-1.5 by numerical simulations using the SPH hydrocode (Jutzi and Michel, 2014). Other estimates (O. Barnouin, presentation at the AIDA meeting, Darmstadt,

February 2014) give a range between 1.3 (resulting in a ΔV of 0.52 mm/s) and 4.1 (ΔV of 1.42 mm/s) for the beta factor, for vertical impacts depending on the assumed internal structure (assuming a 300 kg spacecraft impacting at 6.25 km/s), although most reasonable results range between 1.3-2.0. Note that these estimates do not account for the effect of the target's spin on the outcome.

III.2.3. Environment between and around the two components

We started to investigate the fate of the ejecta using the N-body code pkdrgav adapted to this issue, taking as initial conditions the outcome (ejecta masses/sizes and velocities) computed by impact simulations of the DART impact (see previous sections). The minimum size of the considered ejecta, limited by the resolution of the simulations, is about 10 centimeters. Smaller size ejecta are therefore not accounted for, here, and require another treatment (see below). So far, for practical reasons, we limited our analysis to the fate of ejecta whose vertical velocity is greater than zero and ejection angle greater than 10 degrees above horizon over the first five weeks following their ejection from the target. After about 10 minutes from the impact instant, the particles with the highest speed move at 1.7 km/s (see Fig. 11) and the particles with the lowest speed move at 37 cm/s (with a vertical velocity component of only 3.2 cm/s, i.e. they are ejected near 10 degrees ejection angle). Note that the escape speed of the secondary, assuming a bulk density of 1.3 g/cc and a spherical shape, is about 6.4 cm/s. Consequently, after 5 weeks, none of those particles come back to the secondary but rather escape without any reaccumulation between them. We did not investigate yet the possibility that regolith/loose material in the vicinity of the impact might be affected by the impact event and possibly lift off the surface at speeds comparable to the escape speed. This material, if perturbed by the impact event, may not escape the binary system or take a while to do so, or take a while to come back to the surface. Future investigations will look into this. The influence of the primary was not modeled at the present stage in the dynamics of the ejecta (the secondary was considered isolated). Note that the escape speed from the primary (with assumed bulk density of 1.3 g/cc) at the distance of the secondary is about 20 cm/s, which is still below the minimum speed of the considered ejecta.

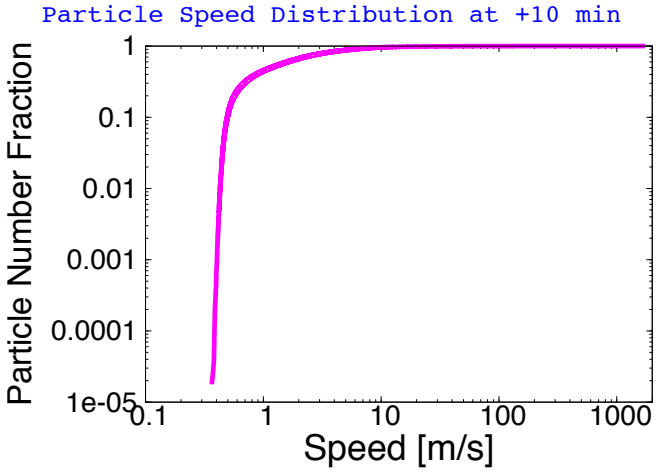

Figure 11: Cumulative number of ejecta as a function of ejection speed computed by numerical simulations using impact conditions similar to those of DART. All ejecta have equal mass, but not equal size as their density differs slightly (from Schwartz

and Michel, 2014). The results are shown at 10 minutes after the impact. Note that most of the ejecta moves at about 40-50 cm/s.

The analysis of the influence of particles smaller than the resolution of the impact simulations (10 cm) needs another kind of modeling. We considered the fate of very small ejecta (micron to cm size particles) by modeling their trajectories with the cometary tail/jets code COSSIM (Vincent et al. 2010). The motion of dust grains in this size range is controlled by the competition between solar gravity and solar radiation pressure, both forces acting in opposite direction and varying with 1/squared distance from the Sun. The ejection velocity of these particles is not well defined so we used in the simulations the worst-case scenario, i.e. dust grains being ejected just above the escape velocity from the secondary. This could lead to particles remaining in the system for a long time, before the radiation pressure pushes them away.

The simulations describe the ejecta cloud as seen from a ground based observatory on Earth, the full extent of the ejecta may not be necessarily visible from the spacecraft (ex: Deep Impact). The impact takes place on 06 October 2022 at 00:00.

We defined arbitrarily a safe distance of 100 km for the spacecraft to be at the time of impact and calculated when particles will leave this volume for different size range (Fig. 12):

1-10 microns:	6 hours
10-100 microns:	1 day
0.1-1 mm:	3 days
1-10 mm :	10 days
1-10 cm :	> 30 days

The brightness of this ejecta cloud depends on the amount of small grains released by the impact and is difficult to estimate. We can compare with the case of asteroid P/2010 A2 (Snodgrass et al. 2010) that presented a dust tail interpreted as the result of an impact by a 5-meter projectile. The larger grains in the ejecta cloud (>mm) remained detectable from Earth more than one year after the event.

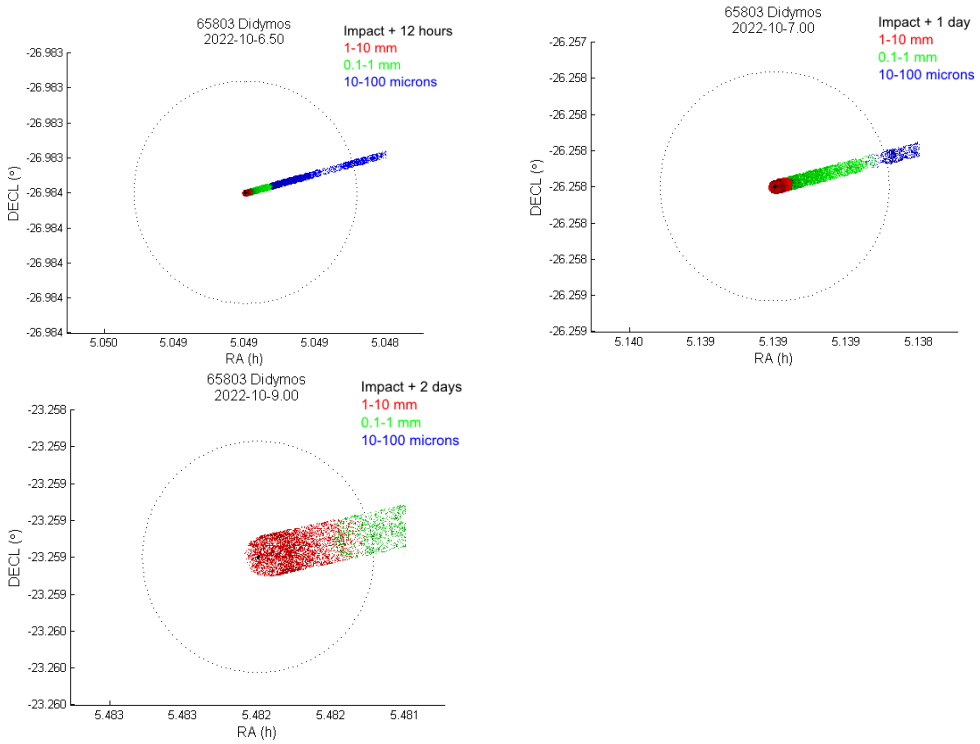

Figure 12: Spatial distribution of dust particles emitted in all directions from the secondary, at speed just above the escape speed. Snapshots are taken at impact + 12 hours, + 1 day, and + 2 days. We considered 3 bins of particle sizes (10-100 microns, 0.1-1 mm, 1-10 mm) represented by different colors. Each size range contains 10 000 particles. The dotted line marks a distance of 100 km from the nucleus.

References

Chesley, S. R., Farnocchia, D., Nolan, M. C., Vokrouhlicky, D., Chodas, P. W., Milani, A., Spoto, F., Rozitis, B., Benner, L. A. M., Bottke, W. F., Busch, M. W., Emery, J. P., Howell, E. S., Lauretta, D. S., Margot, J.-L., Taylor, P. A. (2014). Orbit and Bulk Density of the OSIRIS-REx Target Asteroid (101955) Bennu. ArXiv e-prints, arXiv:1402.5573-

Colwell, J.E., Gulbis, A.A.S., Horanyi, M. & Robertson, S. (2005). Dust transport in photoelectron layers and the formation of dust ponds on Eros. Icarus, 175, 159 – 169.

Colwell, J.E., Batiste, S., Horanyi, M., Robertson, S. & Sture, S. (2007). Lunar surface: Dust dynamics and regolith mechanics. Rev. Geophys., 45.

Delbo, M., Libourel, G., Wilkerson, J., Murdoch, N., Michel, P., Ramesh, K.T., Ganino, C., Verati, C., Marchi, S. (2014). Thermal fatigue as the origin of regolith on small asteroids. Nature, doi:10.1038/nature13153

Halekas, J.S., Delory, G.T., Lin, R.P., Stubbs, T.J. & Farrell, W.M. (2009). Lunar surface charging during solar energetic particle events: Measurement and prediction. J. Geophys.Res., 114.

Harris, A.W., Fahnestock, E.G., Pravec, P. (2009). On the shapes and spins of "rubble pile" asteroids. Icarus, 199, 310-318.

Hughes, A.L., Colwell, J.E. & DeWolfe, A.W. (2008). Electrostatic dust transport on Eros: 3-D simulations of pond formation. Icarus, 195, 630 – 648.
Goertz, C.K. (1989). Dusty plasmas in the solar system. Reviews of Geophysics, 27, 271–292.

Jacobson, S.A., Scheeres, D.J. (2012). Dynamics of rotationally fissioned asteroids: Source of observed small asteroid systems. Icarus, 214, 161-178.

Jutzi, M., Michel, P. (2014). Hypervelocity impacts on asteroids and momentum transfer. I. Numerical simulations using porous targets. Icarus, 229, 247-253.

Lee, P. (1996). Dust Levitation on Asteroids. Icarus, 124, 181–194.

Michel, P. (2013). Physical Properties of Near-Earth Objects that Inform Mitigation. Acta Astronautica, 90, 6-13.

Rozitis, B., Green, S. F. (2013). The influence of global self-heating on the Yarkovsky and YORP effects. Monthly Notices of the Royal Astronomical Society, 433, 603-621.

Rozitis, B., Duddy, S. R., Green, S. F., Lowry, S. C. (2013). A thermophysical analysis of the (1862) Apollo Yarkovsky and YORP effects. Astronomy and Astrophysics, 555, A20.

Schwartz, S.R., Michel, P. (2014). NEOShield study of hypervelocity impacts into small bodies: simulating the fate of ejecta. 45th Lunar and Planetary Science Conference. LPI Contribution No. 1777, p. 2415.

Sickafoose, A.A., Colwell, J.E., Hor´anyi, M. & Robertson, S. (2000). Photoelectric Charging of Dust Particles in Vacuum. Phys. Rev. Lett., 84, 6034–6037.

Snodgrass, C., Tubiana, C., Vincent, J.-B., et al. (2010). A collision in 2009 as the origin of the debris trail of asteroid P/2010 A2. Nature, 467, 814-816.

Vincent, J.-B., Böhnhardt, H., Lara, L.M. (2010). A numerical model of cometary dust coma structures: application to comet 9P/Tempel 1. Astron. Astrophys., 512, A60.

Walsh, K.J., Richardson, D.C., Michel, P. (2008). Rotational break up as the origin of binary asteroids. Nature, 454, 188-191.

Walsh, K.J., Richardson, D.C., Michel, P. (2012). Spin-up of rubble-pile asteroids: disruption, satellite formation, and equilibrium shapes. Icarus, 220, 514-529.

Whipple, E.C. (1981). Potentials of surfaces in space. Reports on Progress in Physics, 44, 1197.

Appendix

DART Requirements
(From the US DART team, may be updated)

The DART mission shall launch a kinetic impactor spacecraft to intercept the secondary member of the binary asteroid 65803 Didymos during its October, 2022 close approach to Earth.

DART shall perform a demonstration of asteroid deflection and measure the change in the binary orbital period to within 10% precision. Note-This measurement is by ground-based observations.

The DART spacecraft shall autonomously target to impact the secondary asteroid through its center of figure. The miss distance from the COF shall be less than 15 m (TBR). Notes-high resolution visible imager for targeting. Miss distance to be refined by analysis.

The spacecraft impact shall be targeted such that the night side of the secondary is illuminated by reflected light from the primary. Note- choice of geometry is to support determination of COF by visible imager.

DART shall determine the impact location within 1 m.

The kinetic impact on the asteroid target shall cause at least a 0.17% change in the binary orbital period.

The kinetic impact shall occur no earlier than September 30, 2022. Goal: the kinetic impact occurs within the Arecibo radar-observing window starting Oct 24, 2022.

Determine local surface topography and geologic context of impact site. Notes- this is to support interpretation of deflection measurement and understanding of kinetic impact effects. This is also a supporting measurement for AIM characterization.